

Published in final edited form as:

*Science*. 2013 May 03; 340(6132): 595–599. doi:10.1126/science.1233936.

## Self-Assembling Cages from Coiled-Coil Peptide Modules

Jordan M Fletcher<sup>1</sup>, Robert L Harniman<sup>1,2,3</sup>, Frederick R H Barnes<sup>1</sup>, Aimee L Boyle<sup>1</sup>, Andrew Collins<sup>1,4</sup>, Judith Mantell<sup>5</sup>, Thomas H Sharp<sup>1,5,#</sup>, Massimo Antognozzi<sup>2,3</sup>, Paula J Booth<sup>5</sup>, Noah Linden<sup>6</sup>, Mervyn J Miles<sup>2,3</sup>, Richard B Sessions<sup>5</sup>, Paul Verkade<sup>5,7</sup>, and Derek N Woolfson<sup>1,5,\*</sup>

<sup>1</sup>School of Chemistry, Cantock's Close, University of Bristol, Bristol BS8 1TS, UK

<sup>2</sup>School of Physics, HH Wills Physics Laboratory, Tyndall Avenue, University of Bristol, Bristol BS8 1TL, UK

<sup>3</sup>Centre for NSQI, Tyndall Avenue, University of Bristol, Bristol BS8 1FD, UK

<sup>4</sup>Bristol Centre for Functional Nanomaterials, Centre for NSQI, Tyndall Avenue, University of Bristol, Bristol BS8 1FD, UK

<sup>5</sup>School of Biochemistry, Medical Sciences Building, University Walk, University of Bristol, Bristol BS8 1TD, UK

<sup>6</sup>School of Mathematics, University Walk, University of Bristol, Bristol, BS8 1TW, UK

<sup>7</sup>School of Physiology and Pharmacology, Medical Sciences Building, University Walk, University of Bristol, Bristol BS8 1TD, UK

### Abstract

An ability to mimic the boundaries of biological compartments would improve our understanding of self-assembly, and provide routes to new materials for the delivery of drugs and biologicals, and the development of protocells. We show that short designed peptides can be combined to form unilamellar spheres approximately 100 nanometers in diameter. The design comprises two, non-covalent, heterodimeric and homotrimeric coiled-coil bundles. These are joined back-to-back to render two complementary hubs, which when mixed form hexagonal networks that close to form cages. This design strategy offers control over chemistry, self-assembly, reversibility and size of such particles.

In viruses (1) and certain bacterial microcompartments (2), capsids and suprastructures are produced via the self-assembly of large folded proteins, usually in highly symmetric manners, and with exquisite positioning of non-covalent protein-protein interactions. Biomimetic assemblies have potential for creating simpler encapsulation systems, and for applications in controlled delivery and release, sensing, and the preparation of protocells for various aspects of synthetic biology (3-5). To these ends, others have produced macroscopic

\*To whom correspondence should be addressed: d.n.woolfson@bristol.ac.uk.

#Present address: Department of Physics, Clarendon Laboratory, Parks Road, University of Oxford, Oxford, OX1 3PU

Supplementary Materials [www.sciencemag.org/](http://www.sciencemag.org/)... Materials and Methods Figs. S1 to S15 Tables S1 to S3 References (25 – 41) Movie S1

“sacs” from peptide amphiphiles (6); and engineered micelle-like structures (7, 8), small polyhedra (9, 10), extended protein arrays (11), and metal-directed assemblies (12, 13) using mainly natural peptides and proteins. Here we show that self-assembled cage-like particles, SAGEs, can be made from a set of short, *de novo*,  $\alpha$ -helical, coiled-coil peptides by employing clear sequence-to-structure relationships and rational-design principles to direct stable and highly specific protein-protein interactions (14-16).

Previously, we developed a toolkit of coiled coils comprising homo-dimer, trimer and tetramers (17), and a number of heterodimers (18). These synthetic peptides, of  $\approx 30$  residues in length, assemble reversibly and form stable structures at micromolar to nanomolar concentrations. To expand this toolkit and to ease the construction of the building blocks for the SAGE design, we engineered two new coiled-coil modules: a shorter ( $\sim 20$  residues) homotrimer (CC-Tri3), and a similarly short obligate heterodimer (CC-Di-AB) comprising acidic (CC-Di-A) and basic (CC-Di-B) sequences (Fig. S1 and Table S1 (19)). We chose a heterodimer for the second module to give control in the following self-assembly process. Our goal was to link copies of CC-Tri3 and CC-Di-A or CC-Di-B through their external surfaces via disulfide bonds (Fig. 1). These covalent constructs, dubbed CC-Tri3—CC-Di-A and CC-Tri3—CC-Di-B, should assemble into complementary trimeric hubs, *hub A* and *hub B*, respectively. Alone, these should be water-soluble, discrete, partly folded helical structures; i.e., CC-Tri3 should spontaneously assemble, leaving CC-Di-A and CC-Di-B orphaned on the outside of the assemblies. Upon mixing, however, the two hubs should co-assemble via association of the CC-Di-A and CC-Di-B modules to produce hexagonal networks with pores of  $\approx 5 - 6$  nm. Because the hubs are flexible and to maximize coiled-coil interactions, we argue that these networks should fold to form closed objects, i.e., SAGEs.

The two coiled coils were synthesized (Fig. S2) and characterized in solution using a combination of circular dichroism (CD) spectroscopy to measure secondary structure, stability, and dissociation constants ( $K_d$  values) (Figs. 2A, S3 and S4, Tables S2 and S3); dynamic light scattering (DLS, Figs. 2B & S5), and analytical ultracentrifugation (AUC, Fig. S6) to probe peptide association. These methods confirmed CC-Tri3 as a highly helical trimeric assembly, with concentration-dependent folding ( $K_{d,20\text{ }^\circ\text{C}} = 3.99 \times 10^{-14} \text{ M}^2$ ), and a midpoint of thermal unfolding ( $T_M$ ) of  $65\text{ }^\circ\text{C}$  at  $50\text{ }\mu\text{M}$  peptide. Similarly, CC-Di-A and CC-Di-B alone were unfolded in the micromolar range, but co-assembled when mixed to form a helical heterodimer, CC-Di-AB, ( $K_{d,20\text{ }^\circ\text{C}} = 5.83 \times 10^{-8} \text{ M}$ ;  $T_M = 51\text{ }^\circ\text{C}$ ) (Table 1). We verified that CC-Tri3 and CC-Di-AB did not form mixed species in the presence of each other by showing that the melting profile of the two coiled coils, when mixed, was the same as the average of the two independent profiles (Fig. S7).

Building toward *hubs A* and *B*, the two-peptide constructs CC-Tri3—CC-Di-A and CC-Tri3—CC-Di-B had reduced mean residue ellipticities (MREs) compared with CC-Tri3 alone. Moreover, these values were close to averages of CC-Tri3 plus either CC-Di-A or CC-Di-B, respectively (Fig. 2A, S3, Table 1). In addition, the melting curves for the hubs were near simple averages of the component curves (Figs. S8 and 9). Next, we mixed three equivalents of CC-Di-A with *hub B*, and of CC-Di-B with *hub A*; i.e., equimolar amounts of the underlying peptide components CC-Di-A and CC-Tri3—CC-Di-B, and of CC-Di-B and CC-

Tri3—CC-Di-A. In both cases, this should produce “terminated”, 9-helix assemblies (Fig. 1). Indeed, the increased MREs observed were indicative of near-complete folding of all of the modules (Figs. 2A and S3, Table 1). Moreover, the thermal denaturation curves for these assemblies were sigmoidal, and the apparent  $T_M$  values measured were near the theoretical value for fully decoupled folding of the CC-Tri3 and CC-Di-AB components of 55 °C (Fig. S9, Tables 1 and S2). In all of these cases, DLS showed that the particle sizes of the peptide modules, hubs and terminated assemblies were  $\approx 2 - 5$  nm, consistent with discrete and appropriately sized objects (Fig. 2B). AUC (Fig. S6) gave solution molecular weights consistent with the compositions of each of the assemblies (Table 1); except for the terminated *hub B*, which had a mass higher than expected, but nonetheless was still a discrete assembly.

These findings all corroborate the modular design approach that underpins the SAGE concept.

When *hub A* and *hub B* were mixed in an equimolar ratio a fine white precipitate formed within minutes, accounting for the >90% of peptide initially in solution. Fresh samples diluted fivefold in PBS and analyzed by DLS indicated particles of hydrodynamic diameter  $132 \pm 42$  nm (Fig. 2C). The role of the disulfide linkage in the assemblies was confirmed by adding the disulfide reducing agent TCEP to the suspension. This ruptured the particles producing smaller structures of diameter  $2.3 \pm 0.9$  nm (Fig. 2C) similar to that observed for a mixture of CC-Tri3 and CC-Di-AB ( $2.5 \pm 0.6$  nm) (Fig. S10).

Scanning electron microscopy (SEM) revealed closed spherical objects of similar diameter ( $97 \pm 19$  nm,  $n = 135$ ) (Fig. 3A, S11). Although the particles appear as aggregates in these particular micrographs, they dispersed in solution (Fig. 2C) and separated when deposited on porous membranes (Fig. S12). Tapping-mode atomic force microscopy (TM-AFM) was performed on particles deposited and dried onto mica. These particles were flattened disks  $9.2 \pm 1.0$  nm thick (averaged from scans over 5 particles) with diameters of  $95 \pm 14$  nm (from 4 measurements each on 5 particles) (Fig. 3, C and D and Fig. S13). As the coiled-coil modules are estimated to be  $\sim 3$  nm in length, the observed thickness of these disks is strong evidence that, in solution, the spheres are hollow and unilamellar rather than being solid, multi-walled, or onion-like structures. That is, they collapse upon drying, presumably releasing water through pores in the assembly. This fits our concept for the SAGEs; i.e., a folded sheet comprising a hexagonal network of peptides (Fig. 1).

Lateral molecular-force microscopy (LMFM) with optical feedback was used in a non-contact regime to explore the assemblies in solution (20). Again, this showed approximately spherical objects (diameter  $79 \pm 12$  nm ( $n = 19$ ); height  $82 \pm 16$  nm (averaged from scans over 6 particles; Fig. 3E). These dimensions are similar to those found by SEM, which should be  $\sim 10$  nm larger because of the sputtered metal coating estimated from the manufacturer’s technical notes to be  $\sim 5$  nm thick (19, 21). Moreover, and intriguingly, the LMFM revealed ultra-structure on the surfaces of the assemblies, notably clear hexagonal shapes, Figs. 4G - I. The edges of the hexagons averaged  $7 \pm 2$  nm ( $n = 22$ ); although such x- and y-dimensions in scanning probe microscopies are tip dependent and are not as reliable as measurements made in z.

Our observations of closed spheres with a tight size distribution, confirmed by three independent methods, is intriguing. It raises two immediate questions: How do the hexagonal networks fold and close, and why are the resulting closed structures so uniform in size?

The first question arises because rigid hexagonal networks should form flat assemblies (like a graphite sheet); and closing a sphere (as illustrated by a football) cannot be achieved with hexagons alone and requires, for example, 12 pentagons. However, the coiled-coil modules and hubs of the SAGEs are more flexible, and the assemblies that they produce may tolerate imperfections required to close. Such imperfections, which are inevitable when closing such structures, could include a few mismatched hub pairings, rather than the perfect hexagonal array shown in Fig. 1.

Closing the particles may be driven by thermodynamic and geometric constraints: Regarding thermodynamics, the hubs are designed to associate with their complementary partners, which has two consequences: (1) hubs from solution co-assemble to grow the network; and (2) these expanding edges have unsatisfied coiled coils, which drive the sheets to close and satisfy as many coiled-coil interactions as possible. In terms of geometry, it is likely there is some intrinsic tendency for the hubs to prefer tripod-like structures, with arms arranged at less than  $120^\circ$  creating curvature. We tested these ideas computationally and experimentally as follows.

Complete SAGEs are too large for atomistic simulations, so we modeled smaller fragments of the hexagonal network. From x-ray crystal structures (17) and standard coiled-coil parameters (22), we generated an array of 19 tessellated hexagons built from CC-Tri3 and CC-Di-AB modules, and with 306 chains in total (Figs. 4A, C). After 5 ns of molecular dynamics (MD) in water, uniform curvature was evident in both the x and y directions (Figs. 4B, D and movie S1). This was reproducible: in this, and multiple MD simulations for smaller 7-hexagon networks, the CC-Tri3 modules remained perpendicular to the curved surface with their *N*-termini always facing “out”.

A sphere of diameter 100 nm has a girth of  $\approx 314$  nm, corresponding to  $\approx 40$  equatorial hexagons. Thus, each hexagon is required to be wedge-shaped subtending an angle of  $\approx 10^\circ$  at the center of the sphere. Further examination of the MD trajectories, and retrospective inspection of the designed sequences suggest a molecular interpretation for this wedging: The disulphide bridges linking the coiled coils are slightly offset towards the *C*-termini; and each peptide has a positively charged lysine residue at the *f* site between these bridges and the *N*-termini (Fig. S1). As borne out by the MD, the positively charged lysine residues repel each other, while the disulfide bonds act as a tether. The overall effect is to splay the collective *N*-termini of each coiled-coil unit apart resulting in wedge-shaped hubs (Fig. S14), producing local and then global curvature.

The question regarding the tight size distribution of the SAGEs is more difficult to rationalize, though this is likely to involve elements such as hub rigidity, the proportion of imperfections required to close a sphere, and entropic factors. To examine how hub rigidity and any preferred local curvature may vary, we analyzed multiple MD simulations of 7-

hexagon tessellates from different starting conditions. After 10 ns simulations, the hub-hub angle approached equilibrium settling to  $33.9 \pm 17.2^\circ$  (Fig. S15). Clearly, the simulations overestimate the local, and therefore, global curvature. Nonetheless, the  $10^\circ$  angle estimated from the experiments is sampled in the simulations (Fig. S15).

To exploit this apparent flexibility, and to test the importance of burying unsatisfied edges en route to closure, we attempted to engineer smaller SAGE particles. We prepared an additional heterodimer module, CC-Di-A1B1 (Table S1). In these peptides, Asn→Ile mutations were made at complementary *a* sites in the hydrophobic face to give a variant with more than two orders of magnitude higher affinity than the CC-Di-AB parent (17); otherwise, we do not expect this change to alter coiled-coil or hub structure or geometry. Thus, the free-energy penalty associated with unsatisfied edges, and proposed to drive closure, should be higher for the variant. When compared by SEM (Fig. 3, A and B), the parent SAGE particles had diameters of  $97 \pm 19$  nm ( $n = 135$ ), whereas those incorporating the variant had diameters of  $68 \pm 12$  nm ( $n = 97$ ) ( $p < 0.001$ ). This translates to the latter having about half the surface area, and provides strong evidence that satisfying coiled-coil interactions on the edge of a growing disk is a key driving force in closing assemblies. Moreover, it illustrates another advantage of our modular design strategy; namely, that altering the  $K_d$  of the individual coiled coils can be used to control SAGE size.

The SAGE concept, though inspired by natural examples, offers routes to closed systems of reduced complexity with the potential for encapsulation. Because the components are modular, interchangeable, and bear termini and side chains that could be derivatized, it should be possible to tune their properties for applications such as vehicles for drug and biomolecule delivery, cages for trapping functional enzyme cascades that allow flux of starting materials and products, components of sensing systems, and as new frameworks for the development of protocells (23).

## Supplementary Material

Refer to Web version on PubMed Central for supplementary material.

## Acknowledgements

We thank the Woolfson group for valuable discussions; the BBSRC for funding to DNW and PJB (BB/G008833/1) and for a studentship to ALB; and the EPSRC for studentships to RLH and THS. JM is supported by a Wellcome University Award. We are grateful to the University of Bristol Advanced Computing Research Centre and the eInfraStructureSouth Consortium for high performance computing; and Jonathan Jones and Electron Microscopy Unit (EMU) School of Chemistry University of Bristol for EM access. The peptides described have been added to the *Pcomp* database for synthetic biology (<http://coiledcoils.chm.bris.ac.uk/pcomp/index.php>).

## References and Notes

1. Lodish, HF. Molecular cell biology. ed. 6th. W.H. Freeman; New York: 2008.
2. Tanaka S, et al. Science. 2008; 319:1083. [PubMed: 18292340]
3. Agapakis CM, Boyle PM, Silver PA. Nat. Chem. Biol. 2012; 8:527. [PubMed: 22596204]
4. Hammer DA, Kamat NP. FEBS Lett. 2012; 586:2882. [PubMed: 22841716]
5. Uchida M, et al. Adv. Mater. 2007; 19:1025.

6. Capito RM, Azevedo HS, Velichko YS, Mata A, Stupp SI. *Science*. 2008; 319:1812. [PubMed: 18369143]
7. Boato F, et al. *Angew. Chem. Int. Ed. Engl.* 2007; 46:9015. [PubMed: 17935102]
8. Raman S, Machaidze G, Lustig A, Aebi U, Burkhard P. *Nanomedicine*. 2006; 2:95. [PubMed: 17292121]
9. King NP, et al. *Science*. 2012; 336:1171. [PubMed: 22654060]
10. Lai YT, Cascio D, Yeates TO. *Science*. 2012; 336:1129. [PubMed: 22654051]
11. Sinclair JC, Davies KM, Venien-Bryan C, Noble MEM. *Nat. Nanotechnol.* 2011; 6:558. [PubMed: 21804552]
12. Brodin JD, et al. *Nat. Chem.* 2012; 4:375. [PubMed: 22522257]
13. Pires MM, Lee J, Ernenwein D, Chmielewski J. *Langmuir*. 2012; 28:1993. [PubMed: 22165843]
14. Bromley EHC, Channon K, Moutevelis E, Woolfson DN. *ACS Chem. Biol.* 2008; 3:38. [PubMed: 18205291]
15. Lupas AN, Gruber M. *Adv. Prot. Chem.* 2005; 70:37.
16. Woolfson DN. *Adv. Prot. Chem.* 2005; 70:79.
17. Fletcher JM, et al. *ACS Synth. Biol.* 2012; 1:240. [PubMed: 23651206]
18. Bromley EHC, Sessions RB, Thomson AR, Woolfson DN. *J. Am. Chem. Soc.* 2009; 131:928. [PubMed: 19115943]
19. See supplementary materials on Science Online.
20. Harniman RL, et al. *Nanotechnology*. 2012; 23
21. [http://www.quorumtech.com/pdf/SputterCoatingTechniques/Sputter\\_coating\\_technica\\_1\\_brief.pdf](http://www.quorumtech.com/pdf/SputterCoatingTechniques/Sputter_coating_technica_1_brief.pdf)
22. Offer G, Sessions R. *J. Mol. Biol.* 1995; 249:967. [PubMed: 7791220]
23. Mansy SS, et al. *Nature*. 2008; 454:122. [PubMed: 18528332]
24. O'Shea EK, Rutkowski R, Kim PS. *Science*. 1989; 243:538. [PubMed: 2911757]

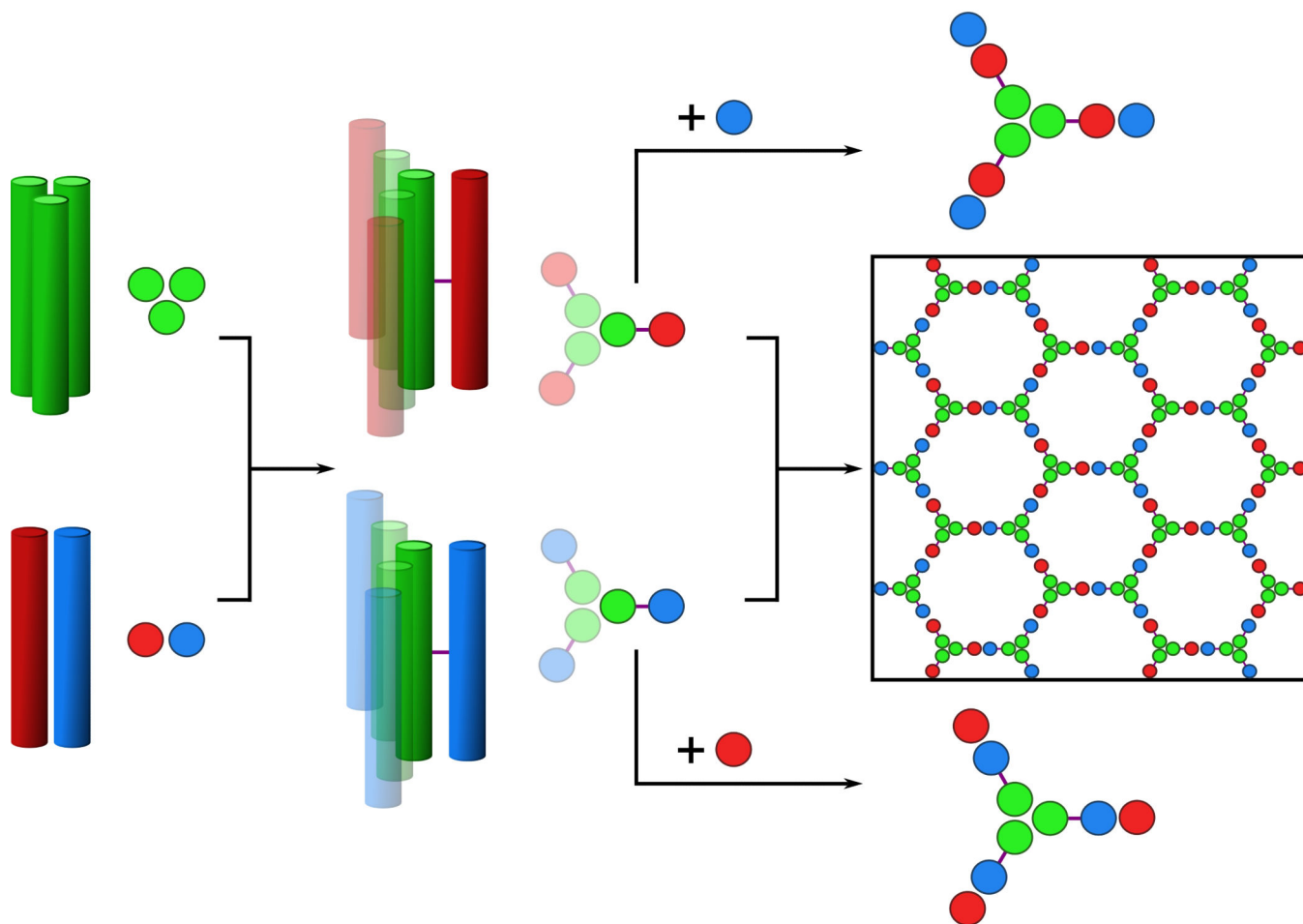


**Fig. 1. Schematics for the design and self-assembly of peptide-based cages**

Left to right: Homotrimeric coiled coil (CC-Tri3, green) and heterodimeric coiled coils (CC-Di-AB); the latter comprises CC-Di-A and CC-Di-B, colored red and blue, respectively. CC-Tri and CC-Di-AB are linked via asymmetric disulfide bonds (purple lines) to render *hub A* (green-red) and *hub B* (green-blue). Mixing *hub A* with CC-Di-B, or *hub B* with CC-Di-A produces discrete 9-helix assemblies; whereas, mixing the hubs directly produces a hexagonal network, which should close.

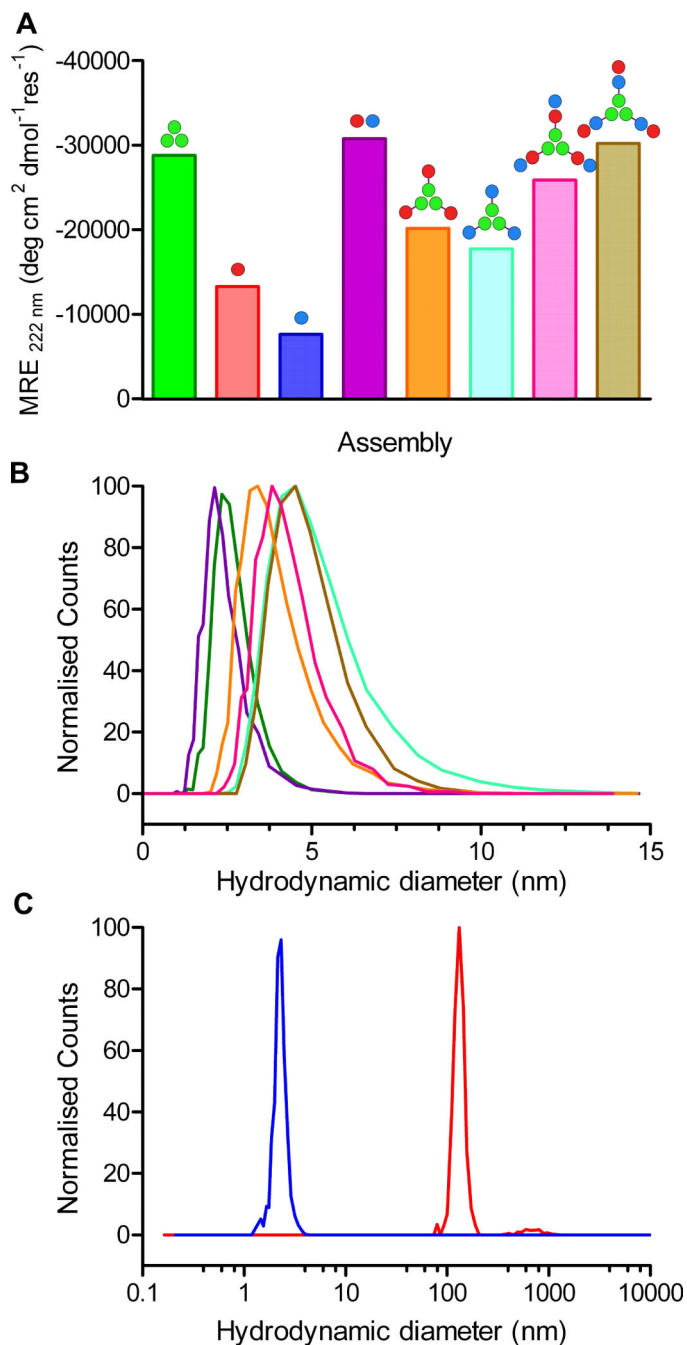


**Fig. 2. Solution-phase characterization of the designed peptide modules, hubs and discrete assemblies**

(A) Mean Residue Ellipticity (MRE) at 222 nm (MRE<sub>222</sub>) from CD spectroscopy in phosphate-buffered saline (PBS) at 20 °C for: CC-Tri3 (50 μM, green); CC-Di-A (50 μM, red); CC-Di-B (50 μM, blue); the mixture of CC-Di-A and CC-Di-B, i.e., CC-Di-AB, (50 μM + 50 μM, purple); *hub A* (CC-Tri3—CC-Di-A, 50 μM, orange); *hub B* (CC-Tri3—CC-Di-B, 50 μM, cyan); *hub A* plus CC-Di-B (50 μM + 50 μM, pink); *hub B* plus CC-Di-A (50 μM + 50 μM, brown). Full CD spectra and thermal denaturation curves are provided in Fig. S3 (19). The leucine-zipper peptide, GCN4-p1, gives a benchmark MRE<sub>222</sub> for 100% α-



helix of  $\approx -36,000 \text{ deg cm}^2 \text{ dmol}^{-1} \text{ res}^{-1}$  (24). **(B)** Hydrodynamic diameters of the coiled-coil modules, hubs and 9-chain terminated assemblies as determined by dynamic light scattering; colors as per panel A. Expanded DLS data are given in Fig. S5. **(C)** DLS data for the assembled SAGE particles before (red) and after (blue) treatment with TCEP (tris(2-carboxyethyl)phosphine).

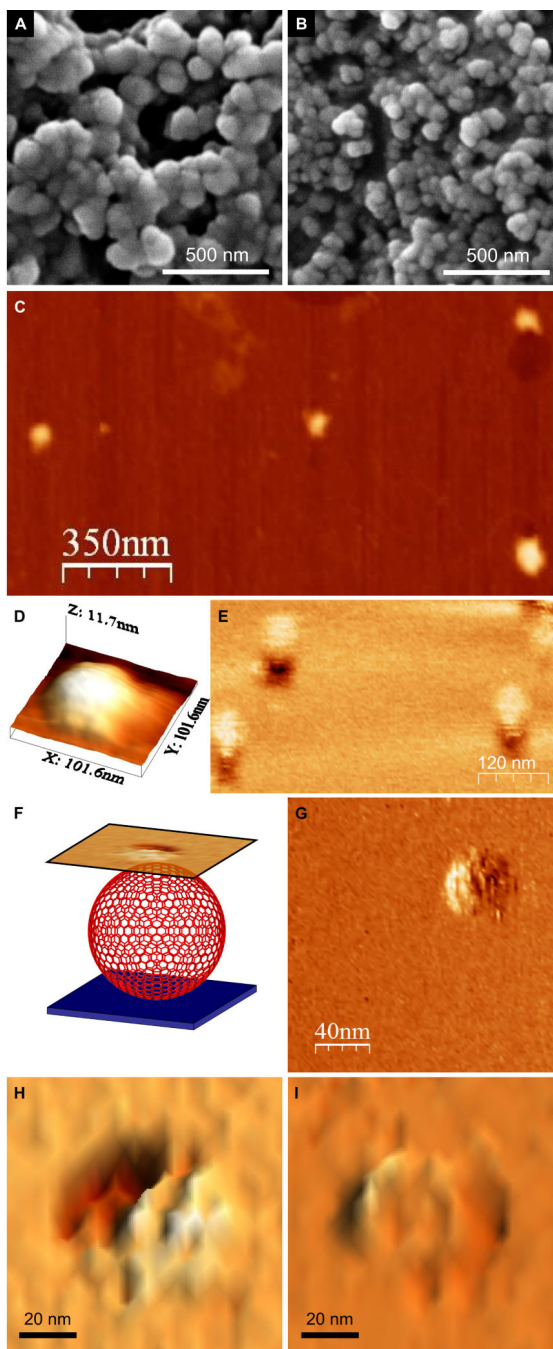
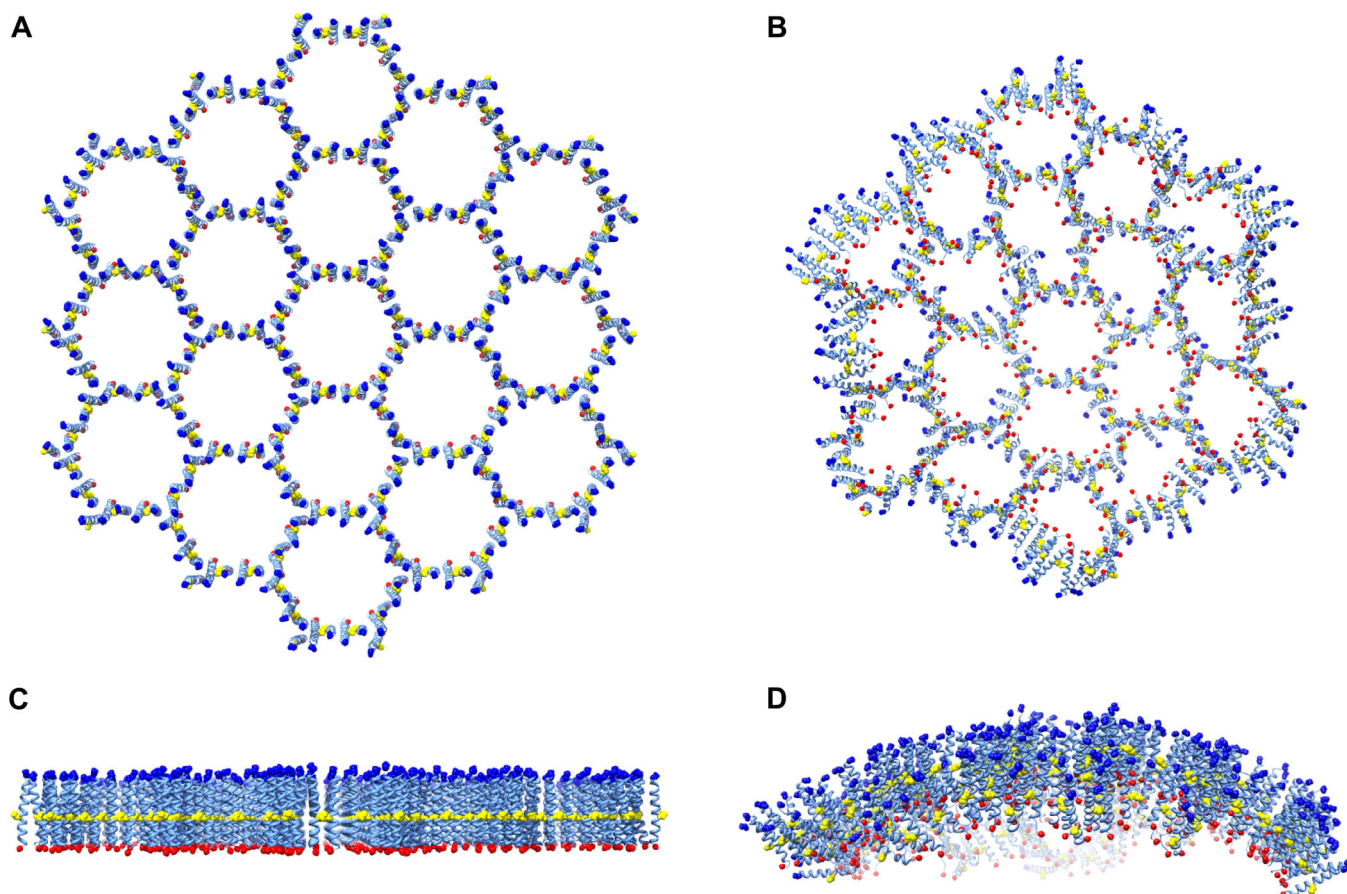


**Fig. 3. (A and B) Scanning electron micrographs of the SAGE particles**  
**(A)** Images recorded after mixing *hub A* and *hub B* in PBS, pH 7.4 (to final concentrations of 50  $\mu\text{M}$  in each of the component peptides, CC-Tri3—CC-Di-A and CC-Tri3—CC-Di-B, *i.e.* 16.7  $\mu\text{M}$  of each *hub*). After 1 h, resuspended material was transferred to a carbon-coated stub and sputter-coated with gold/palladium before imaging. **(B)** Smaller SAGE particles formed by mixing CC-Tri3—CC-Di-A<sub>1</sub> and CC-Tri3—CC-Di-B<sub>1</sub>. Full images are provided in Fig. S11. **(C – I) Scanning probe microscopy of the SAGES.** **(C)** Tapping-mode AFM (TM-AFM) scan of 4 individual collapsed SAGES dried onto a mica substrate.





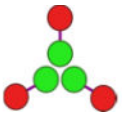
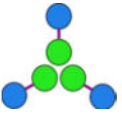
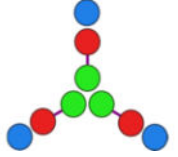
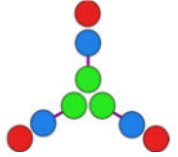
**(D)** 3D representation of the topography measured over a single collapsed SAGE via TM-AFM. **(E)** LMFМ scan recorded in liquid in a noncontact regime with a constant separation of the tip from the glass substrate. **(F)** Schematic representation of the LMFМ scanning regime. An optical feedback maintained the vertically oriented cantilever at a constant separation from the substrate. Mapping the shear-force interaction nanometers above the SAGE allowed an image to be collected in a non-contact mode. **(G – I)** LMFМ images of the hexagonal ultra-structure on the surfaces of hydrated SAGEs.



**Fig. 4. Molecular dynamics of a model for the SAGEs**

(**A** and **C**) Atomistic molecular model of 19 tessellated hexagons comprising *hub A* and *hub B* across three perspectives. These were generated from models for CC-Tri3 and CC-Di-AB aligned “back-to-back” along the 3- and 2-fold symmetry axes and linked through disulfide bonds. As for the synthesized peptides, the termini of the modeled peptides were capped and are represented in blue (acylated *N*-termini) and red (amidated *C*-termini), with the Cys-Cys disulfide linkers colored yellow. (**B** and **D**) Curvature observed following 5 ns molecular dynamics simulations. These were performed under periodic boundary conditions using explicit water (TIP3P) at pH 7 and with 150 mM NaCl present (full details provided as supplementary material (19), along with a movie S1).

**Table 1**  
**Summary of solution-phase biophysical data.**

Assembly		MRE <sub>222</sub> <sup>‡</sup> (deg cm <sup>2</sup> .dmol res <sup>-1</sup> )	T <sub>M</sub> <sup>‡</sup> (°C)	Mass of Assembly by AUC [95% C.I.] (calculated mass)	Hydrodynamic diameter by DLS (nm)
	CC-Tri3	-28,780	65	7,944 Da. [7,858–8,009] (7,960 Da.)	2.6 ± 0.5
	CC-Di-A	-13,294	ND	ND	ND
	CC-Di-B	-7,647	ND	ND	ND
	CC-Di-AB	-30,746	51	5,350 Da. [5,289–5,442] (5,590 Da.)	2.3 ± 0.6
	( <i>hub A</i> ) CC-Tri3— CC-Di-A	-20,168	68	16,910 Da. [16,720–17,110] (16,238 Da.)	3.7 ± 0.6
	( <i>hub B</i> ) CC-Tri3— CC-Di-B	-17,764	56	15,810 Da. [15,662–15,963] (16,153 Da.)	5.0 ± 0.3
	<i>hub A</i> + CC-Di-B	-25,894	54	24,980 Da. [24,795–25,143] (24,505 Da.)	4.1 ± 0.6
	<i>hub B</i> + CC-Di-A	-30,218	57	31,690 Da. [31,574–31,793] (24,505 Da.)	4.7 ± 0.2

<sup>‡</sup>Mean residue ellipticity (MRE) observed at 222 nm, 20 °C.

<sup>‡</sup>Midpoint, or point of inflection, in sigmoidal thermal unfolding curves recorded as the change in MRE<sub>222</sub> whilst ramping the temperature from 5 to 90 °C at 40 °C/hour. All biophysical data were obtained from samples of 50 μM concentration of each peptide component listed, and in PBS at pH 7.4.